Nuclear Materials and Energy 37 (2023) 101539

Contents lists available at ScienceDirect

Nuclear Materials and Energy

journal homepage: www.elsevier.com/locate/nme

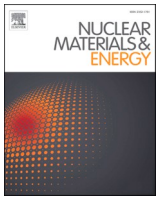

FIB line marking as a tool for local erosion/deposition/fuzz formation measurements in ASDEX Upgrade during the He campaign

M. Rasiński [a,*], S. Brezinsek [a], A. Kreter [a], T. Dittmar [a], K. Krieger [b], M. Balden [b], P. de Marne [b], R. Dux [b], M. Faitsch [b], A. Hakola [c], J. Likonen [c], E. Tsitrone [d], V. Rohde [b], ASDEX Upgrade Team [1], EUROfusion MST1 Team [2]

[a] Forschungszentrum Jülich GmbH, Institut für Energie- und Klimaforschung – Plasmaphysik, 52425 Jülich, Germany
[b] Max-Planck-Institut für Plasmaphysik, 85748 Garching b. München, Germany
[c] VTT Technical Research Centre of Finland Ltd., P.O. Box 1000, FI-02044 Espoo, Finland
[d] CEA, Institute for Research on Fusion by Magnetic confinement, 13108 Saint-Paul-Lez-Durance, France

ARTICLE INFO

Keywords:
FIB line marking
W fuzz He plasma
ASDEX Upgrade
Microstructure
Erosion and re-deposition

ABSTRACT

Tungsten (W) is the prime candidate for the plasma facing material in present and future fusion devices. When exposed to a plasma containing He ions, W can exhibit creation of sub-surface nano-bubbles leading to formation of nano-tendrils called fuzz. Formation of W fuzz was confirmed by many laboratory experiments including He loading in linear plasma devices. There is, however, limited experience related to the parameter space for fuzz formation and re-erosion in a tokamak environment. For this reason, a dedicated experiment was carried out in ASDEX Upgrade (AUG) during its 2022 He campaign to study the evolution of fuzz-like W structures.

Twelve tungsten samples were mechanically polished to a mirror-like surface finish. Six of them were subsequently exposed to a He plasma in the PSI-2 linear device in order to establish a fuzz layer with a thickness of 600 – 800 nm. Before exposure in AUG, all samples were pre-characterized by Focused Ion Beam (FIB) cross-sectioning. In total 48 FIB cross-sections with line markings for quantification of local erosion, deposition and fuzz formation were prepared – 4 on each sample. The samples were placed in two parallel poloidal rows spanning a range of 20 cm around the outer strike line position (OSP). They were subsequently exposed in AUG to a series of 14 consecutive discharges, 8 in H-mode and 6 in L-mode.

Detailed analysis by means of electron microscopy revealed on the samples regions of erosion, deposition and fuzz formation. Below the H-mode OSP, homogeneous co-deposits containing W and O, with a thickness up to 400 nm, were found. In the close vicinity of the H-mode OSP, significant erosion of pre-exposure PSI-2 fuzz was observed. The erosion reached up to 100 – 250 nm, depending on the location. In addition, the initially polished samples did not show any newly formed fuzz in that zone. Above the H-mode OSP, new fuzz was formed with a thickness of up to 1 μm. There was no Mo found in the newly formed fuzz. Pre-exposure PSI-2 fuzz was either removed or modified.

1. Introduction

Tungsten (W) is characterised by a high melting point and high thermal conductivity and correspondingly a high resistance to thermal and particle fluxes. W has also relatively low sputtering yield as well as low retention of hydrogen isotopes [1]. For that reasons W is employed in current fusion devices as JET [2], ASDEX Upgrade (AUG) [3] or WEST [4] as a divertor and first wall plasma facing material (PFM). In future fusion devices such as ITER [5] or DEMO [6], it is also foreseen to use W as PFM, especially in the divertor region.

When exposed to a plasma containing He ions, on the surface of W hair-like structures called “fuzz” can be formed. The full mechanism of fuzz formation is not yet completely understood, but it is considered to involve several processes, including creation of nano-bubbles and their

* Corresponding author..
E-mail address: m.rasinski@fz-juelich.de (M. Rasiński).
[1] See author list of U. Stroth et al. 2022 Nucl. Fusion 62 042006.
[2] See author list of B. Labit et al. 2019 Nucl. Fusion 59 086020.

https://doi.org/10.1016/j.nme.2023.101539
Received 6 August 2023; Received in revised form 29 September 2023; Accepted 11 October 2023
Available online 13 October 2023

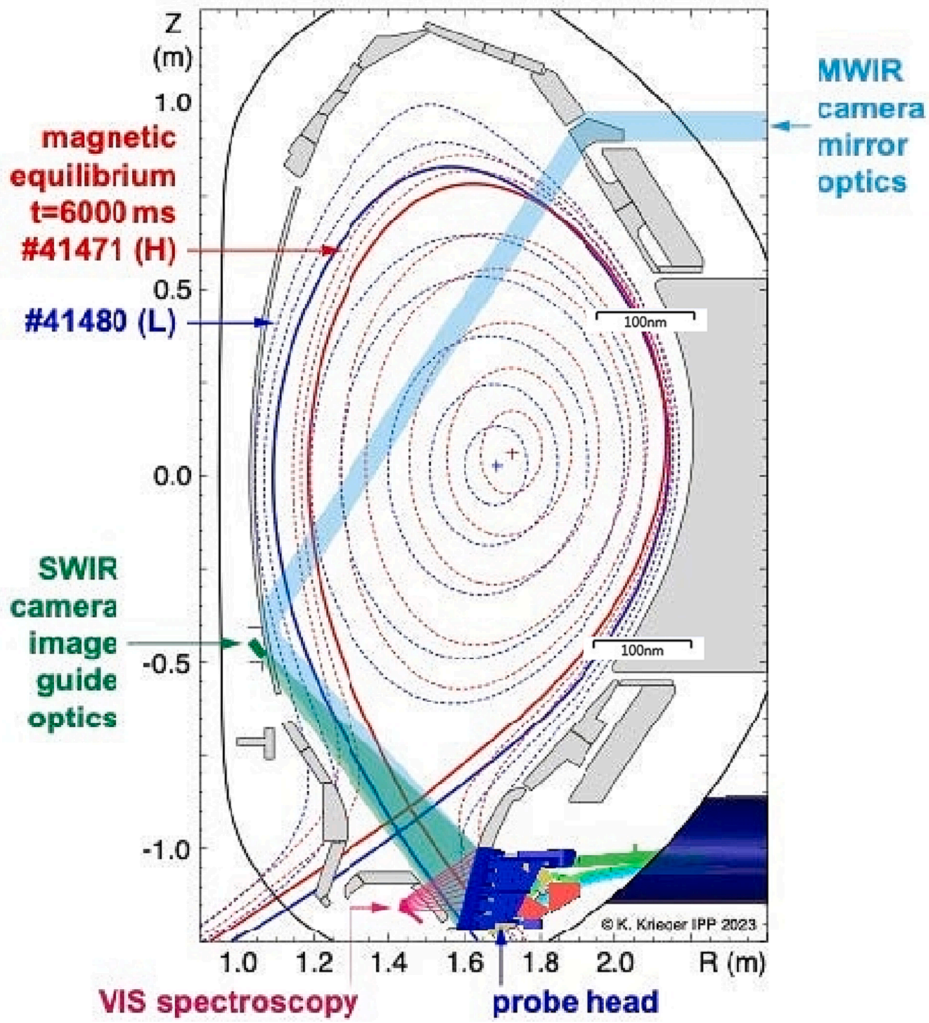

Fig. 1. Poloidal cross-section of ASDEX Upgrade: divertor manipulator for samples exposure (probe head) and viewing lines of the optical spectrometers onto the probe head are marked. Additionally, the magnetic equilibrium for H-mode (red) and L-mode discharges (blue) are indicated. (For interpretation of the references to colour in this figure legend, the reader is referred to the web version of this article.). (For interpretation of the references to colour in this figure legend, the reader is referred to the web version of this article.)

coalescence beneath the surface [7]. Summary of a current state of fuzz growth understanding can be found elsewhere [8]. Fuzz formed on the surface of W exhibits different properties with respect to erosion, thermal conductivity or H isotopes retention. For that reason, it is very important to know its properties as well as fuzz formation conditions under given operation conditions of a fusion device.

The formation of tungsten fuzz was widely studied in many linear plasma devices [910111213], which lead to a general description of conditions required for fuzz formation. Essential parameters for fuzz formation are: (i) W surface temperature (T_{surf}) in the range 1000 to 2000 K, (ii) He ion fluence greater than 2×10^{24} ions/m^2 (also for the He fraction in a mixed plasma exposure) and (iii) He ion energy greater than 20 eV [11]. It is also known that the presence of molybdenum (Mo) may affect the W fuzz formation conditions, namely by reducing the required $T_{surf.}$ [14]. For that reason, it is important to avoid Mo contamination when investigating the W fuzz evolution.

Despite a vast amount of experimental results from linear plasma devices, there is still limited experience on W fuzz formation in fusion devices. There have been attempts to study the growth of fuzz in tokamaks and stellerators such as Alcator C-Mod [15], AUG [16171817], LHD[19], WEST [20] or JET. Up to now no pure W fuzz was obtained for several reasons. Alcator C-Mod was equipped with plasma facing components made of both Mo and W so that the created fuzz was an admixture of W and Mo [15]. A similar issue arose in an experiment during the AUG He campaign in 2019. A set of W samples was mounted in a dedicated target tile made of molybdenum-based allow with addition of titanium and zirkonium (TZM) for exposure with the divertor manipulator. As a consequence, the grown fuzz contained up to 20 at. % of Mo [18]. During the WEST dedicated He campaign, no W fuzz-like structures were observed, although the main criteria for W fuzz formation were fulfilled [20]. These examples clearly show that the conditions for W fuzz formation in a tokamak are much more complex than in a linear device. Criteria like W erosion and re-deposition as well as fuzz annealing present during tokamak exposure are expected to play a significant role, and cannot be studied in linear devices.

In view of previous experiments, the attempt to study W fuzz in fusion devices under well-defined conditions is important, particularly aiming at a reduced presence of impurity species. This paper presents results from AUG during the He campaign 2022 where for the first time formation of pure W fuzz layers (without any Mo contamination) could be studied.

2. Experimental

A set of twelve W samples with a size of $33 \times 12 \times 5$ mm^3 were mechanically polished to obtain a mirror like surface finish. Six of them

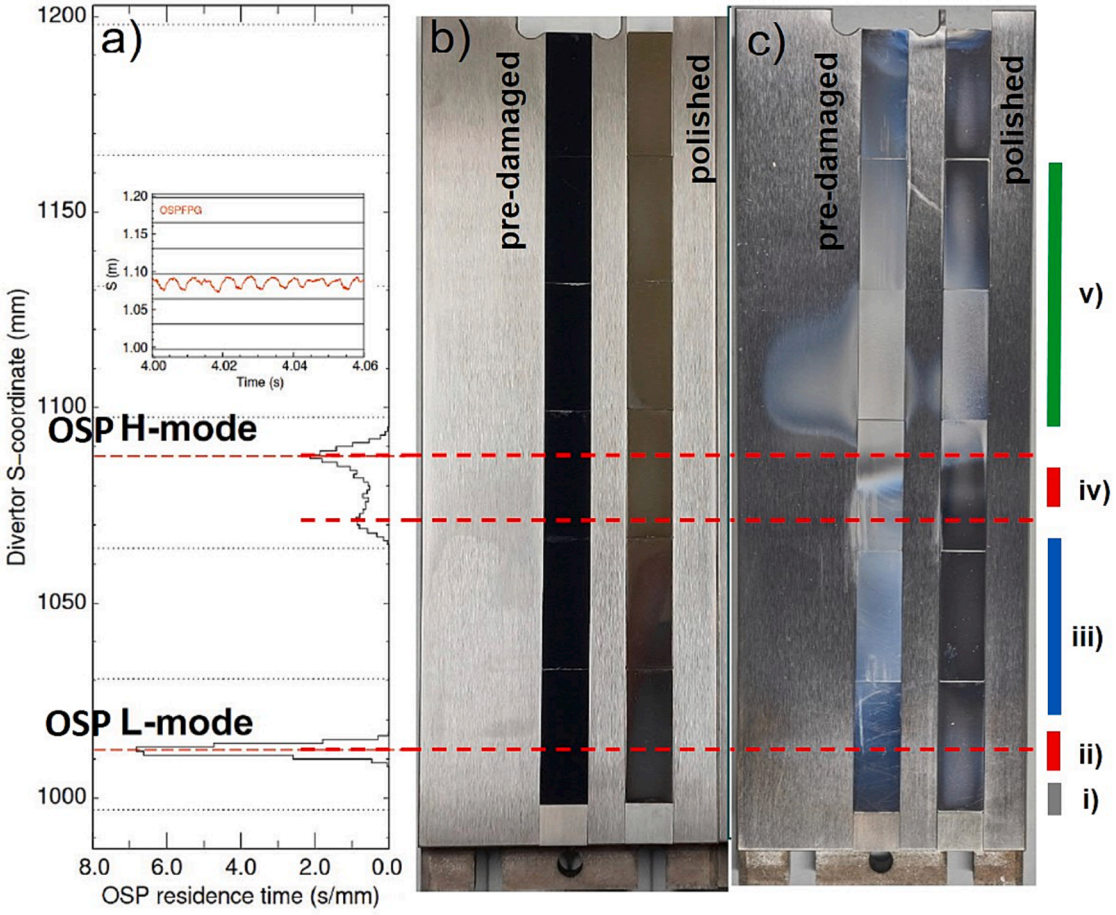

Fig. 2. Images of DIM-II W tile with the installed samples before (b) and after (c) AUG He plasma exposure. Diagram (a) illustrates the local distribution of the integrated OSP residence time across the tile versus the divertor S-coordinate system. The maxima represent the position of L-mode and H-mode outer strike-line position (OSP). The later one was modulated as the insertion indicates.

were subsequently exposed to He plasma discharges in the PSI-2 linear device. Details of the experimental setup of PSI-2 are described in [21]. A bias voltage of − 100 V was applied to the samples, resulting in an incident ion energy in the range of 60——80 eV. The incident ion flux was in the range of 8.4×10^{21} $m^{-2}s^{-1}$ and the incident ion fluence was 1.5×10^{25} m^{-2}. The surface temperature, T_{surf}, during plasma exposure was in the range 1150 – 1200 K. In the following, the samples with W fuzz created in PSI-2 will be named "pre-damaged".

The surface morphology of the samples before and after plasma exposure was analysed using a field emission scanning electron microscope (FE-SEM) [Zeiss Crossbeam 540]. A dual beam scanning electron microscope/focused ion beam (SEM/FIB) device, equipped with an energy dispersive X-ray analyser (EDX) [Oxford Instruments X-Max 80] was used for surface imaging, cross-section preparation, TEM lamella preparation, cross-section imaging and elemental composition analysis. For each sample four FIB cross-sections were prepared, two in the centre and two in a corner of each sample. Each cross-section was rotated in a way that the analysed side of a cross-section was facing in a different direction. Moreover, on each cross-section, additional line markings were created using a 10 pA FIB beam of 30 keV Ga ions. The line markings, consisting of five lines spaced every 1 μm, served as a distinct reference for local erosion and re-deposition measurements. In particular cases, when the line marking system was covered by co-deposition, additional gentle cleaning with a 50 pA and 30 keV Ga beam was used to make the marker visible again.

The pre-characterised samples were subsequently mounted as inserts in two dedicated tungsten target tiles for exposure with the AUG DIvertor Manipulator (DIM-II) [22]. Fig. 1 shows the poloidal cross-section of AUG with the two plasma equilibria and the geometries of both the manipulator probe head and local diagnostics used in the experiment. The samples were installed in the tiles in two vertical rows, with the pre-damaged samples in one row and the polished samples in the adjacent row. Fig. 2 (c) shows a photo of the tile with installed samples before AUG He exposure and (b) a photo of the retrieved tile after AUG He exposure.

The samples were exposed in two regimes of local plasma conditions, by executing two series of L-mode and H-mode discharges, respectively. The two scenarios were spatially separated on the tile by adjusting the outer strike point location (OSP) between the two discharge series as shown in Fig. 1. Apart from the OSP position, both scenarios were executed in the same magnetic configuration at identical plasma current (I_p = 0.8 MA) and toroidal magnetic field (B_t = -2.5 T). The H-mode discharges were heated with neutral beam injection (NBI, P_{NBI} = 6 MW) and central Electron Cyclotron Resonance Heating (ECRH, P_{ECRH} = 4 MW). For the L-mode discharges the heating power was reduced to P_{ECRH} = 1 MW without NBI heating.

The local distribution of the integrated OSP residence time across the tile is shown versus the divertor S-coordinate in Fig. 2a. The S-coordinate system presents poloidal trajectory following the divertor tile surface in millimetres. Note that the S-coordinate is used later in the paper as an indicator for position and orientation of given images. In the first eight discharges the H-mode plasma scenario was used with the OSP located on the third sample counted from the bottom of the tile. Due to an instability in the plasma control system, the OSP oscillated over the sample in a range of ≈20 mm. The total ion fluence near OSP in the H-mode discharge series derived from Langmuir probe measurements

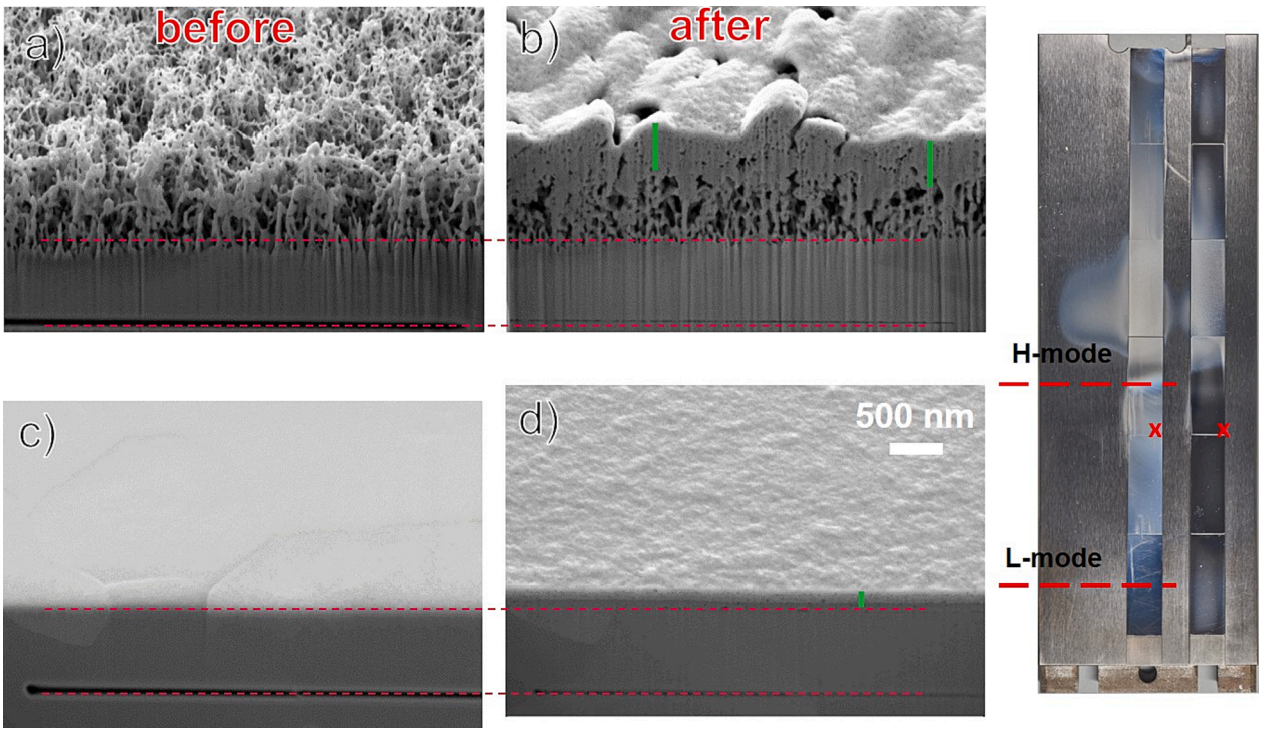

Fig. 3. SEM images of FIB-prepared cross-section with line marking before (a, c) and after (b, d) AUG He plasma exposure of the "pre-damaged" (a,b) and the polished samples (c,d) at S = 1067. The red dashed lines highlight the position of the FIB marker lines and the surface edge. Green lines indicate the region where the co-deposited layer was formed. Photo of DIM-II W tile with mounted samples after AUG exposure with red × marking the position on the sample were the images are coming from. (For interpretation of the references to colour in this figure legend, the reader is referred to the web version of this article.). (For interpretation of the references to colour in this figure legend, the reader is referred to the web version of this article.)

reached values of 3.4 × 10^{24} m^{-2} assuming He^{2+} as dominant plasma ion species. Further away from the OSP (sample positions 4 and 5) the ion fluence was falling off to ≈2 × 10^{24} m^{-2}. In the subsequent five discharges the L-mode scenario was used with the OSP moved down to the middle of the lowest samples. Near OSP the total ion fluence in these discharges was a factor 10 smaller at ≈0.3 × 10^{24} m^{-2}.

During the H-mode discharges the local surface temperature of the samples was measured by analysis of their IR emission, which was recorded by a thermography camera viewing the two tiles exposed with the divertor manipulator through an image guide optics at the central column (see Fig. 1). Because of the glass fibres used for image transmission, the observation was limited to the Short Wavelength Infra-Red (SWIR) spectral range around 1.7 μm. The camera system was calibrated directly after the campaign by a calibrated tungsten filament lamp installed at the manipulator tile position. The derived time evolution of the apparent surface temperature (assuming a tungsten emissivity of ε = 0.1) at the centre and edges of the samples is shown in.

Fig. 7. Unfortunately, adaptive exposure time control was not yet implemented in the camera acquisition software so that in the hottest areas the camera saturated at an apparent surface temperature of 1800 K, with actual temperatures estimated to reach values above 2500 K near OSP.

3. Results and discussion

The visual changes induced by the plasma exposure of the samples are illustrated by Fig. 2, which shows the tungsten tile with installed samples before b) and after (c) AUG He plasma exposure. Already this initial impression suggests significant modification of the surface morphology by the incident He ion particle and power load. Based on the observed surface evolution and the cross-section morphology changes, the position of the samples across the tile can be divided into 5 regions, namely (i) below the L-mode OSP, (ii) near the L-mode OSP, (iii) in-between L-mode and H-mode OSPs, (iv) near the H-mode OSP and (v) above the H-mode OSP. Each region is characterised by a different surface modification pattern resulting from the corresponding variation of He plasma-surface interaction. Each region is also schematically marked in the Fig. 2.

(i) Below the L-mode OSP.

Below the L-mode OSP, near the lower edge of the tile, the surface morphology of both polished and pre-damages samples remains untouched. Structure and thickness of the pre-damage W-fuzz are preserved with no visible changes. The surface of the polished sample shows no indication of He induced damage. The prepared FIB line markings on both cross-sections (pre-damaged and polished) confirm that neither erosion nor co-deposition occurred at this location.

(ii) Near the L-mode OSP.

The surface of the samples close to the L-mode OSP is visibly smoothened. FIB-prepared cross-sections reveal local erosion. The top part of the pre-damage fuzz is removed, but the near-surface regions remains untouched. However, it is difficult to measure exactly the eroded amount of the fuzz structure because of its inhomogeneity. The measured local erosion on the polished surface was in the range of 50 nm at most for an accumulated He^{2+} fluence from the L-mode discharges of ≈0.3 × 10^{24} m^{-2}.

(iii) In-between L-mode and H-mode OSP.

The region in-between the two OSP locations is characterized by visible smoothening of the sample surface after exposure. Pre-damage fuzz is completely covered by deposited material. FIB cross-sections confirm the existence of a co-deposition layer containing W and O, with thickness varying depending on the location on the tile. Fig. 3 shows SEM images of the cross-section before (a, c) and after (b, d) AUG plasma exposure in the location where the thickness of co-deposited layer is the largest. Green lines indicate the region where the co-deposited layer was formed. The thickness reached 100 nm and 250 nm for polished (Fig. 3d) and pre-damaged sample (Fig. 3b),

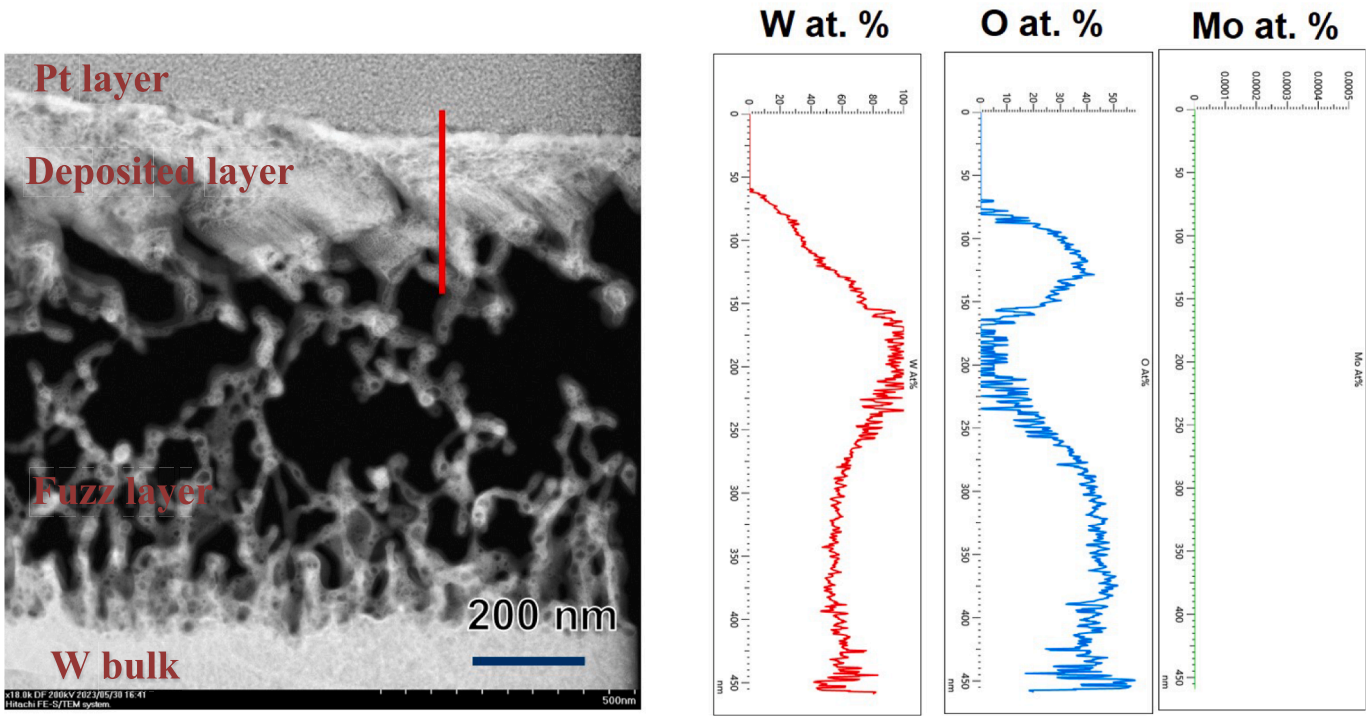

Fig. 4. STEM image of PSI-2 pre-damaged sample after AUG He plasma exposure. The sample was placed in-between H-mode and L-mode OSP at S = 1067 mm where highest re-deposition rate was observed. EDX line scan across marked red line are attached illustrating the distribution of W, O and Mo in at. %. Material above the surface is the Pt coating layer coming from FIB thin lamella preparation. (For interpretation of the references to colour in this figure legend, the reader is referred to the web version of this article.). (For interpretation of the references to colour in this figure legend, the reader is referred to the web version of this article.)

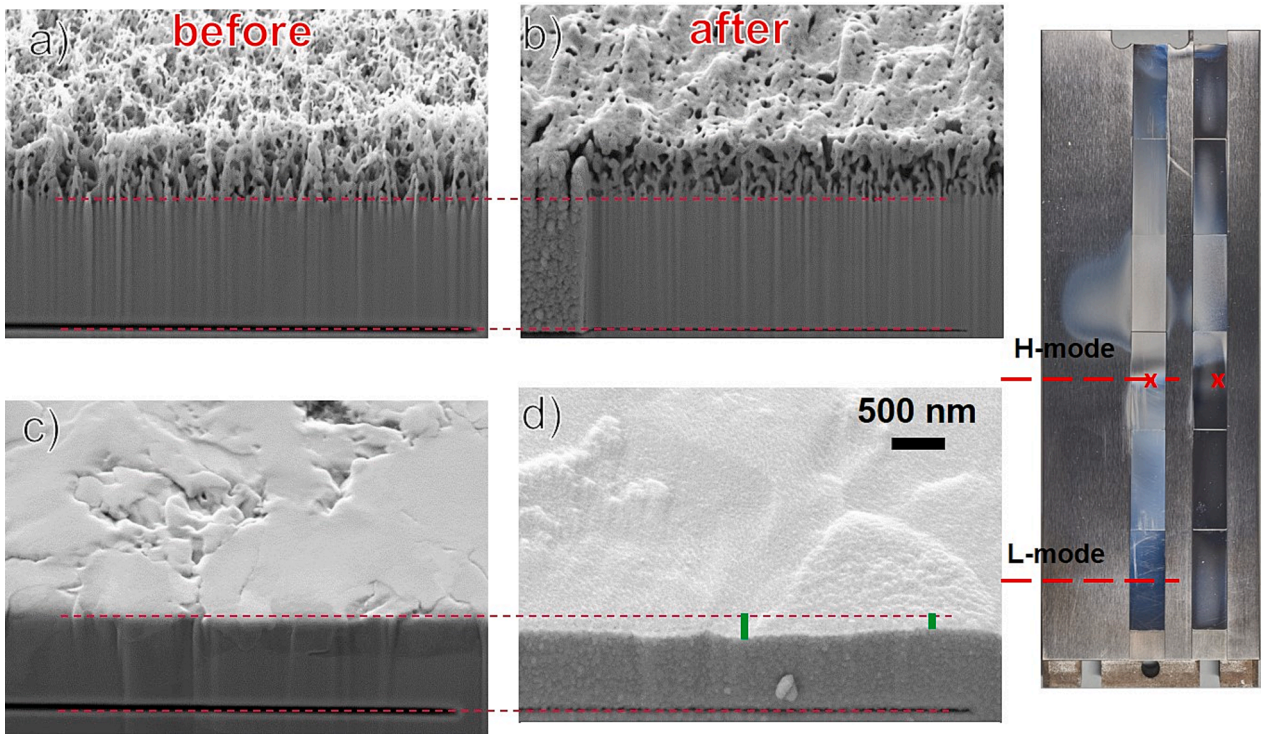

Fig. 5. SEM images of FIB-prepared cross-section with line marking before (a, c) and after (b, d) AUG He plasma exposure at S = 1080 mm. Green lines indicate the region where the local erosion was measured. Photo of DIM-II W tile with mounted samples after AUG exposure with red × marking the position on the sample were the images are coming from. (For interpretation of the references to colour in this figure legend, the reader is referred to the web version of this article.). (For interpretation of the references to colour in this figure legend, the reader is referred to the web version of this article.)

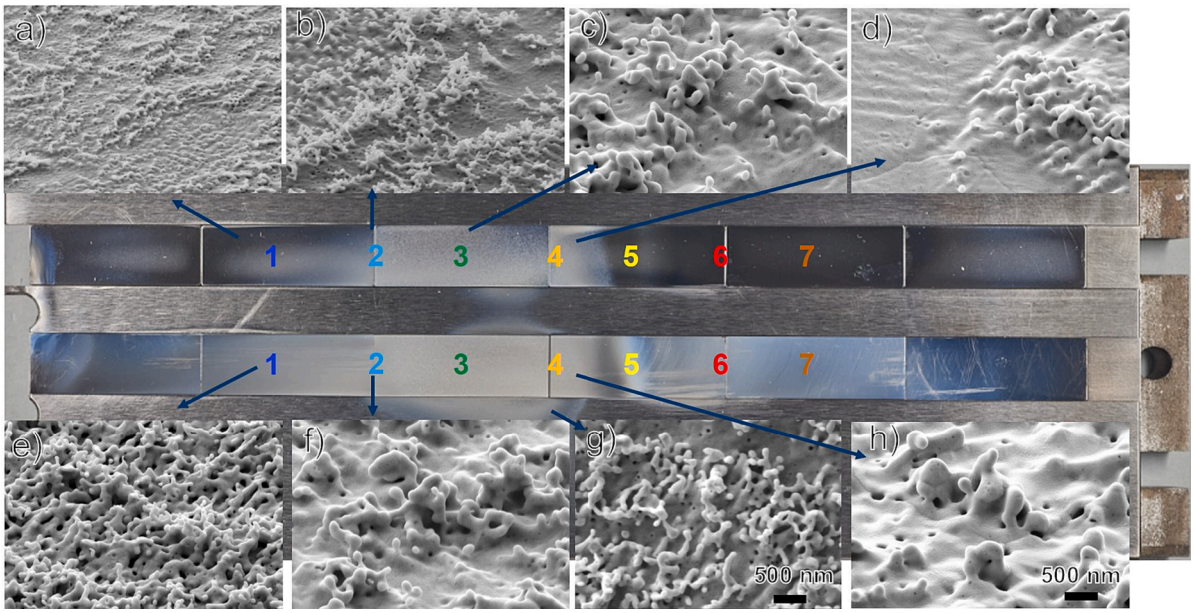

Fig. 6. SEM surface images of polished (a-d) and pre-damaged (e, f and h) samples after AUG He plasma exposure. Different structures of formed W fuzz depending on the exposure position are observed. The fuzz formation on the surface of DIM-II W file is also presented (g).

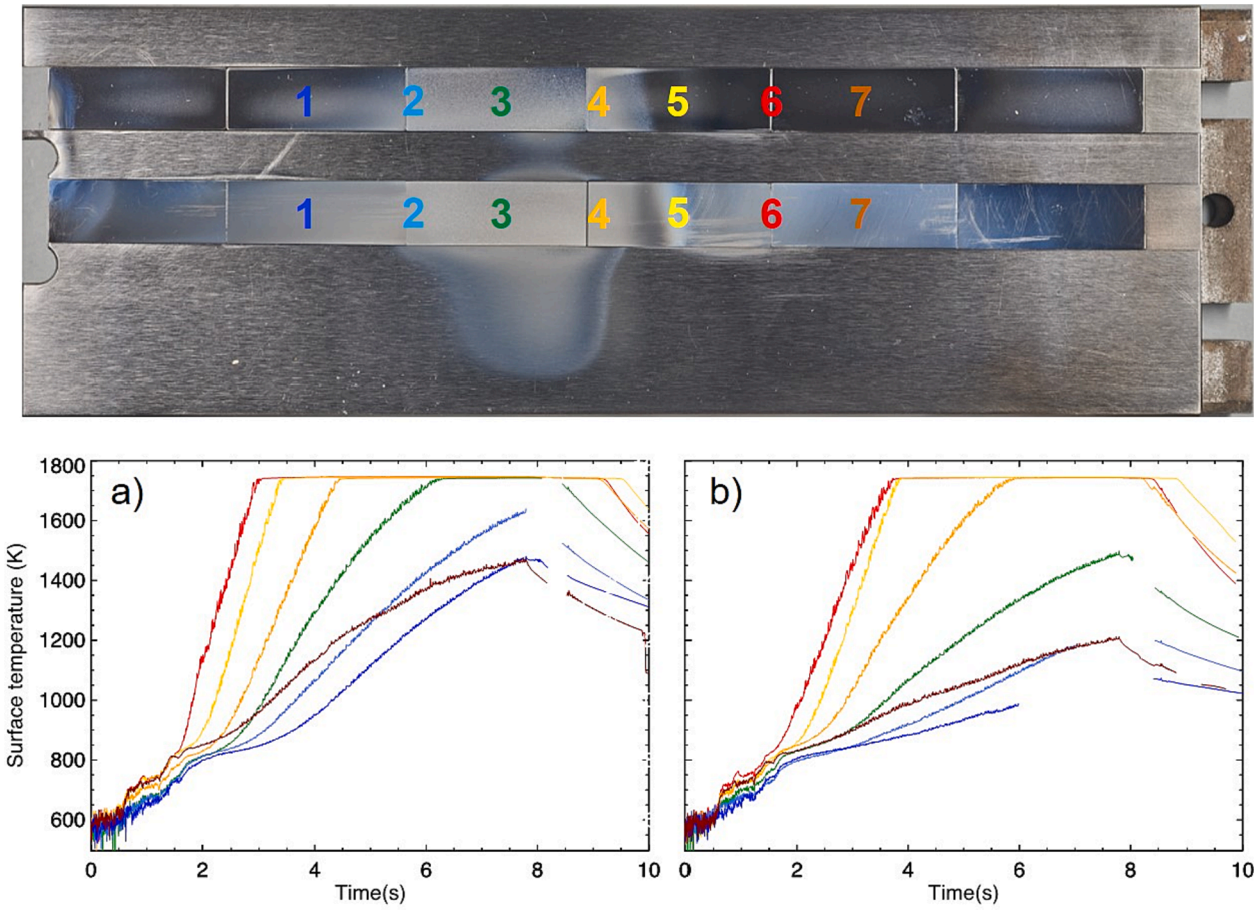

Fig. 7. Apparent surface temperature evolution during H-mode discharge #41473 for a) pre-damaged and b) polished set of samples based on SWIR camera. The positions of the measurements are indicated by coloured numbers. These colours correspond to the colour of the temperature graphs.

respectively. Below the co-deposition layer, pre-damaged fuzz shows no significant modifications. The structure of the co-deposited layer is porous, as illustrated in Fig. 4. The figure shows the STEM image of the pre-damaged sample with the co-deposited layer after exposure. The structure of pre-damage fuzz tendrils is porous, containing He nano-bubbles. The red line indicated the position of EDX line scan for

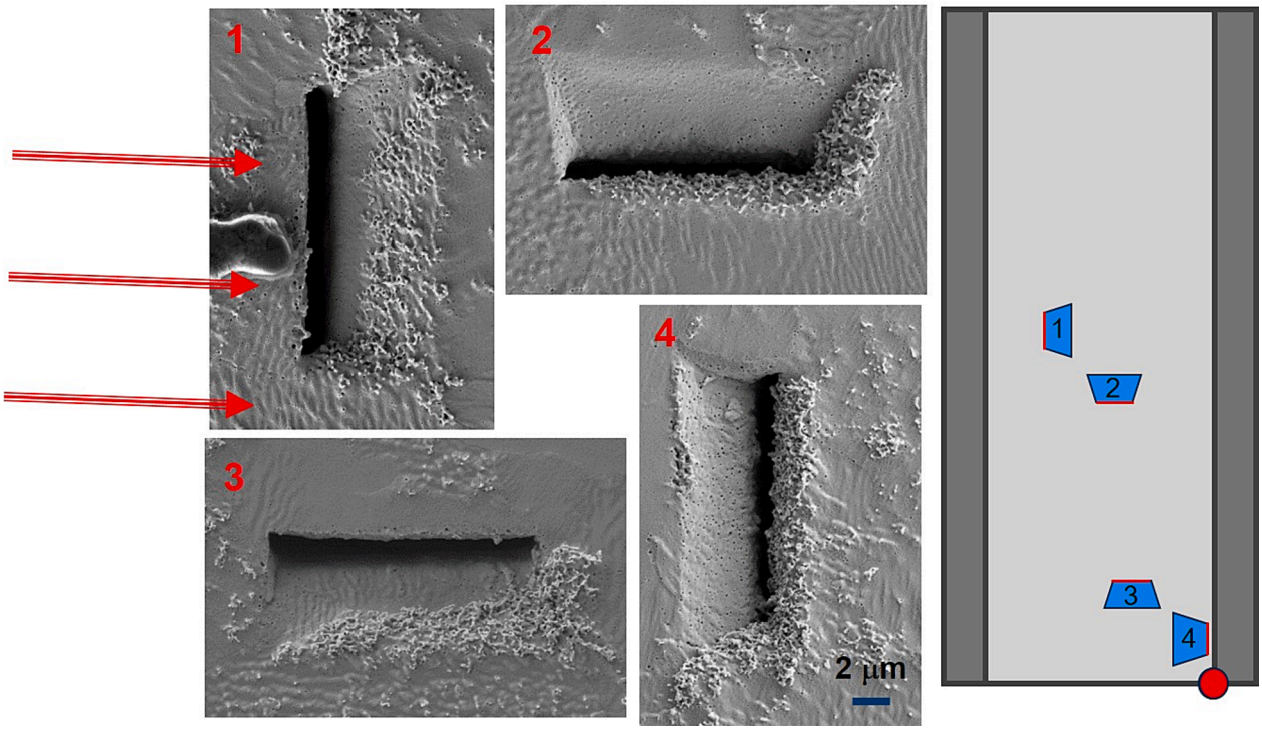

Fig. 8. SEM images of the FIB-prepared cross-sections oriented as they were cut on the sample at S = 1114 mm (1, 2) and at S = 1100 mm (3, 4). Sample was exposed above the H-mode OSP where new W fuzz was formed. Red arrows indicated the direction of the plasma. W fuzz formation inside the FIB trenches corresponding to plasma direction is visible. (For interpretation of the references to colour in this figure legend, the reader is referred to the web version of this article.). (For interpretation of the references to colour in this figure legend, the reader is referred to the web version of this article.)

chemical analysis together with given intensity profiles of W, O and Mo along the line. Apart from W, the deposited layer contains at most 40 at. % of O. No trace of Mo was found. The porous structure of deposits formed during AUG discharges is very similar to those previously reported [23].

(iv) Near the H-mode OSP.

Fig. 5 presents SEM images of the FIB-prepared cross-sections before (a, c) and after (b, d) AUG plasma exposure. The top surface of the pre-damaged fuzz is collapsed whereas the polished sample reveals a typical erosion pattern. The bottom part of the pre-damage fuzz is preserved, as its inner structure looks the same before and after AUG plasma exposure. Green lines indicate the erosion rate which was calculated based on the FIB line markings. The local erosion reached 150 – 250 nm depending on the grain orientation of the substrate. Different grains exhibited different erosion rate [24]. The accumulated He^{2+} fluence in the complete L-mode and H-mode discharge series near the H-mode OSP reached 3.4×10^{24} m^{-2}. The incident He ion energy during the inter-ELM is in the range 80 – 160 eV. On the other hand, according the free streaming model the ELM ions should arrive at the target plate still at their pedestal energy, which for AUG would be 500 – 1000 eV. The sputtering threshold energy for He in W is approximately 110–120 eV [25]. The measured erosion is by that caused by both inter-ELM He ions (having the energy greater that the sputtering threshold) as well as the intra-ELM ions.

(v) Above the H-mode OSP.

In the region above the H-mode OSP, the formation of new W-fuzz was observed. The created fuzz is neither uniform nor homogenous on both polished and pre-damages samples. Pre-damaged fuzz from PSI-2 is removed and partly converted into new W-fuzz. Fig. 6 presents SEM images of the surface of samples exposed above the H-mode OSP. The bottom row shows pre-damaged samples and the top row the adjacent polished samples. Different fuzz structures, depending on the position on the tile are visible for both polished and pre-damaged samples. With decreasing distance to the OSP the fuzz tendrils appear coarser. Positions further away from the OSP shows formation of finer fuzz structures. The fuzz formation was also observed on the DIM-II W tile (Fig. 6g). Moreover, He bubble formation can be seen in-between the fuzz tendrils.

Since the accumulated fluence above the H-mode OSP is only slowly falling off from.

3×10^{24} m^{-2} to 2×10^{24} m^{-2}, the differences in the morphology of the new W fuzz can be rather attributed to the locally varying surface temperature during the discharge. Fig. 7 presents apparent surface temperatures during single H-mode shot number 41,473 with temperature values derived from SWIR camera IR intensities. The temperature evolution is shown at both pre-damaged (a) and polished (b) samples for different positions on the tile, as indicated with coloured numbers. The colour of the numbers at a given position corresponds to the colour of the temperature time trace in the graphs. Formation of new W fuzz was observed at positions 1–4, with 5 being the location of the OSP. As discussed above, the camera measurement saturated for temperatures > 1800 K. Local camera saturation occurred at position 3, and 4 for pre-damaged samples and at location 4 for polished samples. For similar values of T_{surf} (for example 3 polished and 2 pre-damaged – around 1500 K) a similar structure of the formed fuzz is observed. The same is seen for position 1 polished (top row) and 2 pre-damaged (bottom row), where the measured temperature was 1400 K and 1250 K, respectively. This demonstrates a very clear dependency of the structure of formed fuzz from T_{surf}. The lowest measured temperature at position 1 for polished samples was around 1000 K just above the sensitivity threshold of the camera. There, local fuzz formation with tendril thickness below 40 nm and height below 200 nm was observed.

Fig. 8 shows SEM images of FIB-prepared cross-sections above the H-mode OSP where new fuzz was formed. T_{surf} at this position was saturated at the camera above 1800 K (position 4 on the top row of polished samples). The presented orientation of cross-sections was as they were machined on the samples. Red arrows indicate the direction of the incident He plasma flux. The SEM analysis shows here local fuzz formation inside the FIB trenches with the position where the fuzz is

formed inside each trench clearly corresponding to the plasma direction.

4. Conclusions

Polished and pre-damaged (in the linear plasma device PSI-2) samples were exposed to subsequent series of identical H-mode and L-mode He plasma discharges in AUG. Each sample contained four FIB-prepared cross-sections with additional line markings for detailed, local measurement of erosion/deposition and fuzz formation and evolution. Below the OSP of the L-mode discharges no visible surface modification occurred. Near the OSP locations, in both L-mode and H-mode, local erosion was found. In-between the two OSP locations, deposited layers consisting of W and O and with a thickness up to 250 nm were observed. Above the H-mode OSP location, formation of new W fuzz was observed on both pre-damaged and polished samples as well as on the adjacent W tile. Fuzz formation was very non-uniform and strongly dependent on surface temperature. The fuzz thickness reached values of up to 1 μm and the single tendril thickness varied depending from the location on the sample and hence T_{surf}. With decreasing distance to the H-mode OSP, T_{surf} increased and by that thicker W fuzz tendrils were formed. No trace of Mo in the newly created W fuzz was observed, demonstrating that for the first time formation of Mo free W fuzz could be studied under tokamak He plasma exposure conditions.

CRediT authorship contribution statement

M. Rasinski: Conceptualization, Methodology, Formal analysis, Investigation, Writing – original draft, Visualization. **S. Brezinsek:** Conceptualization, Resources, Project administration, Funding acquisition. **A. Kreter:** Formal analysis, Investigation. **T. Dittmar:** Formal analysis, Investigation. **K. Krieger:** Conceptualization, Resources, Project administration, Formal analysis, Writing – review & editing. **M. Balden:** Formal analysis, Investigation, Writing – review & editing. **P. de Marne:** Formal analysis, Investigation. **R. Dux:** Formal analysis, Investigation. **M. Faitsch:** Formal analysis, Investigation. **A. Hakola:** Conceptualization, Resources, Project administration, Funding acquisition. **J. Likonen:** Conceptualization, Resources, Project administration, Funding acquisition. **E. Tsitrone:** Conceptualization, Resources, Project administration, Funding acquisition. **V. Rohde:** Formal analysis, Investigation.

Declaration of Competing Interest

The authors declare that they have no known competing financial interests or personal relationships that could have appeared to influence the work reported in this paper.

Data availability

Data will be made available on request.

Acknowledgement

“This work has been carried out within the framework of the EUROfusion Consortium, funded by the European Union via the Euratom Research and Training Programme (Grant Agreement No 101052200 — EUROfusion). Views and opinions expressed are however those of the author(s) only and do not necessarily reflect those of the European Union or the European Commission. Neither the European Union nor the European Commission can be held responsible for them.”

References

[1] G. Pintsuk, Tungsten as a Plasma-Facing Material Reference Module in Comprehensive Nuclear Materials vol 4 (2012) 551–581.
[2] V. Philipps, et al., Fus. Eng. Design 85 (2010) 1581–1586.
[3] R. Neu, et al., Journal of Nuclear Materials 438 (2013) S34–S41.
[4] J. Bucalossi, et al., Nuclear Fusion 62 (2022) 042007.
[5] R.A. Pitts, et al., Journal of Nuclear Materials 438 (2013) S48–S56.
[6] J.H. You, et al., Nucl. Mater. Energy 16 (2018) 1–11.
[7] S. Kajita, Journal of Nuclear Materials 418 (2011) 152–158.
[8] J.A.R. Wright, Tungsten 4 (2022) 184–193.
[9] M. Baldwin, et al., Nuclear Fusion 48 (2008) 035001.
[10] S. Möller, et al., Physica Scripta T170 (2017) 014017.
[11] S. Kajita, et al., Nuclear Fusion 49 (2009) 095005.
[12] S. Kajita, et al., Journal of Nuclear Materials 548 (2021) 152844.
[13] T.J. Petty, et al., Nuclear Fusion 55 (2015) 093033.
[14] M.I. Patino, et al., Physica Scripta T171 (2020) 014070.
[15] G.M. Wright, et al., Nuclear Fusion 52 (2012) 042003.
[16] S. Brezinsek, et al., Nucl. Mater. Energy 12 (2017) 575–581.
[17] A. Hakola, et al., Nuclear Fusion 57 (2017) 066015.
[18] M. Balden et al., Microscopy study of the growth and erosion of fuzz on tungsten by helium plasma exposure on ASDEX Upgrade, 24th International Conference on Plasma Surface Interactions in Controlled Fusion Devices (PSI 2020), virtual, 25 Jan 2021 - 29 Jan 2021.
[19] M. Tokitani, et al., Nucl. Mater. Energy 12 (2017) 1358–1362.
[20] E. Tsitrone, et al., Nuclear Fusion 62 (2022) 076028.
[21] A. Kreter, et al., Fusion Science and Technology 68 (2015) 8.
[22] A. Hermann, et al., Fus. Eng. Design 98 (2015) 1496.
[23] M. Rasinski, et al., Fus. Eng. Design 86 (2011) 1753–1756.
[24] K. Schlueter, et al., Physical Review Letters 125 (2020) 225502.
[25] W. Eckstein, Sputtered Energy Coefficient and Sputtering Yield, IPP report 17/29 (2011).